Quiescence and Self-Renewal of Stem Cells ¬require a Type 2-Deiodinase mediated cell-autonomous surge in intra-cellular Thyroid Hormone signalling

Maria De Stefano
University of Naples Federico II
Raffaele Ambrosio
IRCSS SDN
Cristina Luongo
Department of Clinical Medicine and Surgery, University of Naples Federico II
Tommaso Porcelli
University of Naples https://orcid.org/0000-0002-6162-5819
Giuseppina Mancino
University of Naples Federico II
Feliciano Visconte
CEINGE Biotecnologie Avanzate Scarl, Naples, Italy
Daniela Di Girolamo
University of Naples Federico II
Emery Di Cicco
University of Naples
Caterina Miro
University of Naples Federico II
Caterina Missero
Center for Genetic Engineering, Napoli, Italy
Monica Dentice
Department of Clinical Medicine and Surgery, University of Naples Federico II
Domenico Salvatore (domsalva@unina.it)
University of Naples https://orcid.org/0000-0002-4556-7620

Article

Keywords:

Posted Date: January 28th, 2022

DOI: https://doi.org/10.21203/rs.3.rs-1258078/v1

Abstract

Stem cells are critical for the regeneration and homeostasis of adult tissues. Thyroid hormone (TH), whose intracellular concentration is increased by Type 2 deiodinases (D2), is implicated in multiple cell functions. While reduced TH levels play a role in muscle stem cell activation, nothing in known about the role of TH in quiescence. Here we show that D2 is specifically expressed and marks quiescent stem cells in muscle and skin and increases intracellular TH. Acute D2-depletion in quiescent muscle stem cells triggers their spontaneous transition from G_0 into a G_{Alert} state. Upon muscle injury, D2-depletion increases the proliferative potential of activated precursor cells but impairs self-renewal of progenitors returning to quiescence. Genetic D2-depletion leads, in the long run or upon multiple injuries, to depletion of the stem cell pool and regenerative failure. Mechanistically, D2-produced TH sustains Notch signalling by directly promoting the expression of Notch receptors and their canonical target genes. In normal and pathological settings, transient drug-induced D2 blocking accelerates muscle regeneration and skin wound healing. In conclusion, a D2-induced increased in intracellular TH concentration is critical in maintaining stem cell quiescence and in regulating self-renewal. In this context, tissue-specific manipulation of TH may be an innovative therapeutic tool in the field of regenerative medicine.

Highlights

- **D2 is a novel marker of quiescent stem cells in both muscle and skin, and its action customizes thyroid hormone metabolism during quiescence.**
- **D2 controls the quiescence and self-renewal state in muscle by sustaining Notch signaling.**
- **Genetic cell-specific D2-depletion is sufficient to induce transition from G_0 to G_{Alert} state.**
- **Drug-induced D2-blocking can be exploited to accelerate the expansion of stem cell progenitors in response to injury, in both muscle and skin.**

Introduction

Stem cells sustain continuous tissue homeostasis by generating tissue progeny while self-renewing through cell division (Brack and Rando, 2012; Feige et al., 2018; Wang and Rudnicki, 2011). This process is necessary to ensure continuous tissue maintenance in various organs, and most of the stem cell properties, namely quiescence, self-renewal, and differentiation are controlled by the stem cell microenvironment (Fuchs and Blau, 2020; Fuchs et al., 2004; Rudnicki et al., 2008; Tumbar et al., 2004; Yin et al., 2013).

The intracellular thyroid hormone (TH) concentration is regulated by the action of the deiodinase enzymes, three seleno-proteins named D1, D2, and D3 (Ambrosio et al., 2017; Bianco et al., 2019; Gereben et al., 2008; Luongo et al., 2019). In particular, D1 and D2 convert the pro-hormone thyroxine (T4) into the active hormone T3. Conversely, D3 converts T3 (triiodothyronine) to T2 (diiodothyronine) and T4 to rT3 (reverse triiodothyronine), both products are considered as almost inactive thyroid hormone metabolites.

We had previously demonstrated that a D3 surge and the consequent reduction of TH is necessary for the activation and expansion of activated muscle stem cells (Dentice et al., 2014). Following activation, D3 declines while D2 surge at the end of the myogenic process, increasing intracellular T3 which is required to allow proper cell differentiation (Dentice et al., 2014; Dentice et al., 2010). D3 is not expressed in quiescent stem cells and whether and how the regulation of thyroid hormone action occurs in this cell context is completely unknown.

Thyroid hormone also plays an important role in skin homeostasis (Paus, 2010; Slominski and Wortsman, 2000; Slominski et al., 2002). Clinical evidence (Bodo et al., 2009; van Beek et al., 2008) and studies conducted in hypothyroid mice and rats suggest that TH is involved in epidermal proliferation and differentiation, hair growth, and wound healing (Safer et al., 2001). These findings implicate TH in the regulation of stem cell function, in both muscle and in skin (Contreras-Jurado et al., 2014; Safer et al., 2005).

Significant progress has been made toward elucidating the signals involved in the regulation of adult stem cells and tissue homeostasis (Yin et al., 2013). Among other important functions, it is now well established that the Notch signalling pathway plays a role in maintaining stem cells of various tissues in a quiescent state (Bjornson et al., 2012). In particular, Notch signalling is crucial in the control of stem cells homeostasis also by exerting its action in the self-renewal process (Baghdadi et al., 2018; Wen et al., 2012) (Fujimaki et al., 2018). Despite significant progress, the precise molecular mechanisms governing the quiescent state of stem cells are poorly understood. In this context, a relevant step forward was the identification of an intermediate state between G_0 and G_1 phase of the cell cycle, designated "G_{Alert}" in which stem cells are more rapidly poised to enter the cell cycle in response to injury (Rodgers et al., 2014). This phase is induced by the circulating Hepatocyte Growth Factor activator released by a distal muscle injury, for example in the contralateral leg (Rodgers et al., 2017).

The aim of this study was to evaluate whether and how TH signalling is involved in the control of stem cell quiescence. We identified D2 as a novel marker of quiescence in different contexts. Using inducible genetic models to ablate the *Dio2* gene specifically in stem cells, we demonstrate that TH-producing D2 maintains the quiescence state in muscle and skin and regulates stem cell self-renewal. We provide evidence that in muscle this function is achieved through sustained Notch signalling. Moreover, D2-depletion leads to transition of the dormient-quiescent muscle stem cell to a G_{Alert} state, which significantly accelerate upon injury the activation of MuSCs and tissue repair.

In conclusion, here we describe a novel pathway by which TH metabolism regulates homeostasis, cell self-renewal and regenerative potential in the stem cell compartment in various tissues. This process requires a cell autonomous mechanism able to rapidly modulate intracellular T3 concentration and adapt it to the varying metabolic needs occurring in stem cells.

CONTACT FOR REAGENT AND RESOURCE SHARING

Further information and requests for resources and reagents should be directed to and will be fulfilled by the Lead Contact, Domenico Salvatore (domsalva@unina.it).

Experimental Model And Subjiect Details

Animals

Animals were house and maintained in the animal facility at CEINGE Biotecnologie Avanzate, Naples, Italy. Tg:Pax7-nGFP, Tg:Pax7^{CreERT2} and R26^{mTmG} mice were kindly provided by Shahragim Tajbakhsh (Pasteur Institute, Paris, France) (Mourikis et al., 2012), Dio2$^{fl/fl}$ (Luongo et al., 2015), D2-3xFLAG (Castagna et al., 2017), *mdx* (dystrophic muscle) mice (Anderson et al., 1994), global-D2KO (Christoffolete et al., 2007) were used in this study. Gt (ROSA)26Sor$^{tm1(Notch1)Dam}$/J and C57BL/6 were purchased from The Jackson Laboratory (Stock No: 008159 and 000664 respectively) Tg:K14-Cre^{ERT} mouse was previously described (Miro et al., 2019). All mice used for experiments were adults, between 12-16 weeks of age while the *mdx* mice used were between 12- 50 weeks of age as indicated. Both sexes were used for experiments as indicated. Animals were genotyped by PCR using tail DNA.

Animal study approval

Experiments and animal care were conducted in accordance with institutional guidelines. All animal studies were conducted in accordance with the guidelines of the *Ministero della Salute* and were approved by the Institutional Animal Care and Use Committee (IACUC: 167/2015-PR and 354/2019-PR).

Cell cultures and reagents

C2C12 were obtained from ATCC. Proliferating cells were cultured in Dulbecco's modified Eagle's medium (DMEM) (Microgem, AL007-500ML) supplemented with 20% Fetal Bovine Serum (FBS) (Microgem, RM10432-500ML), 2mM glutamine (Gibco, #25030024), 50 i.u. penicillin and 50µg/ml streptomycin (Gibco, #15070063) at 37°C. To induce differentiation, cells at 70% confluence were switched from 20% FBS to 2% horse serum (HS) (Gibco, #16050122) and Dulbecco's modified Eagle's medium supplemented with 10µg/ml insulin (Sigma Aldrich, I2643) and 5µg/ml transferrin (Sigma Aldrich, T8158).

METHODS

Animal procedures

Tamoxifen (TAM) (Sigma Aldrich, T5648) was dissolved in corn oil (Sigma Aldrich, C8267)/10% ethanol (Carlo Erba, #4146052) at a concentration 10 mg/ml. Mice were injected intraperitoneally with TAM for five consecutive days (80 mg/Kg of body weight) for experiments involving inducible Cre^{ERT2}. To evaluate *in vivo* cell proliferation, animals were administrated 10 mg/ml Bromodeoxyuridine (BrdU) (Sigma Aldrich, B5002) in drinking water or were injected intraperitoneally with EdU (Sigma Aldrich, #900584) at 2.5mg/ml as indicated in the Results section.

Fluorescence activated cell-sorted MuSCs

Cells were isolated by FACS from Tg:Pax7-nGFP mice as previously described (Rocheteau et al., 2012). In brief, limb muscles were dissected and minced in ice-cold DMEM. Samples were then incubated with a mix of 0.1% collagenase A (Sigma Aldrich, C9891), 0.2% Dispase II (Roche, #04942078001) and 2.5mM $CaCl_2$ for 30 minutes at 37°C in shaking water bath. After digestion DMEM was added to the muscle suspension and filtered, through a 70-µm cell strainers (Corning, #431751), then spun at 50g for 10 min at 4°C to remove large tissue fragments. The supernatant was collected and washed twice by centrifugation at 600 g for 15 min at 4°C. Before fluorescence-activated cell sorting (FACS), the final pellet was resuspended in cold DMEM and 1% penicillin-streptomycin supplemented with 2% FBS, and the cell suspension was filtered through a 30-µm strainer (BD Bioscience, #340598). FACS was performed using FACS Aria IIIu (Becton Dickinson) by gating for GFP fluorescence. MuSCs have been cultured in 1:1 DMEM:MCDB (Gibco, 10372019) containing 20% serum FBS, 1% penicillin-streptomycin 2% ultroser^{TM}G (PALL-life sciences, #15950-017). Cells were plated on Matrigel (BD Biosciences; catalog #354234) or collected in a lysis buffer for RNA or protein extraction.

FACS-sorted epithelial stem cells

Dorsal skin was removed from mice and treated with trypsin 0.25% (Sigma Aldrich, T4799) over night after removal of adipose tissue. The epidermal layer was separated from derma, chopped and incubated with trypsin 0.25% for 7 minutes to 37°C. After digestion, FBS was added to sample to inactivate trypsin. The cells were filtered with 70-µm cell strainer. Cell sorting was performed using APC-anti-mouse CD34 (Biolegend, #119310), PE-rat anti human integrin alpha-6 (BD Pharmingen, #555736), upon incubation for 1 hour at room temperature. Fluorescence-activated cell sorting analysis was performed using FACS Aria IIIu (Becton Dickinson).

Single myofiber isolation and culture

Single myofibers were isolated from the Extensor Digitorum Longus (EDL) muscle and incubated with 0.1% collagenase type I (Sigma Aldrich, #C9891) in DMEM for 60-70 minutes at 37°C. Following enzymatic digestion, mechanical dissociation was performed to release individual myofibres that were then transferred in 60-mm fetal bovine serum (FBS) -coated plates in DMEM/ F12 (50%) supplemented with 20% FBS, 1% penicillin-streptomycin (Gibco). Fibers were fixed at different time points after plating fibers were fixed in 4% PFA (Merck, #1.04005.1000) for 10 minutes and stained for specific antibody. For experiments with the chemotherapeutic drug AraC (Cytosine ß-D-arabinofuranoside, Sigma Aldrich, C1768), myofibers were cultured for 72 hours in medium and then incubated with 100 µM AraC for 48 hours and fixed (day 5).

Western Blotting

Muscle stem cells freshly isolated from Tg:Pax7$^{CreERT2/+}$; D2$^{fl/fl}$ (hereafter called cD2KO) or control mice were lysed in radioimmunoprecipitation assay (RIPA) buffer (50 mM Tris-Cl [pH 8.0], 200 mM NaCl, 50

mM NaF, 1 mM dithiothreitol, 1 mM Na3VO4, 0.3% IGEPAL, and a protease inhibitor cocktail (Sigma Aldrich, P8340)). Cells were boiled at 99°C for 5 min and centrifuged for 10 min at 300 rpm. The samples were loaded in each lane onto 10% SDS-PAGE gels followed by Western blotting. The antibodies used are listed in Table S1. Antibody-labeled protein bands were revealed by using the Immobilon Western Chemiluminescent HRP Substrate (Millipore, WBKLS0500). The gel images were analyzed using Image Lab version 5.2.1 (Biorad Laboratories) software

qPCR

Total RNA was extracted from freshly sorted or cultured cells with a Qiagen RNeasy Micro kit according to the manufacturer's instructions (Qiagen, #74004) and then reverse-transcribed into cDNA by using VILO reverse transcriptase (Invitrogen, #11756050) according to the manufacturer's instructions. Quantitative real-time PCR was performed using iQ5 Multicolor Real Time Detector System (BioRad) with SYBR Green Master mix (BioRad, #1708882). Cyclofilin A gene served as the housekeeping gene controls for ΔC_T calculations [ΔC_T = (C_T of the target gene) - (C_T of housekeeping genes)]. The primer sequences we used are listed in Table S2 of the supplemental material. Fold expression values were calculated using the $2^{-\Delta\Delta CT}$ method, where $\Delta\Delta C_T$ = (ΔC_T of the treatment sample) - (ΔC_T of control samples) (with the control value normalized to 1). Three technical replicates were performed for all qPCR experiments.

Chromatin immunoprecipitation (ChiP) assay

Mouse C2C12 myoblasts were cross-linked with 1% formaldehyde in culture medium for 10 min at RT after which cells were scraped into SDS lysis buffer. The cells were further sonicated and diluted for immunoprecipitation with the indicated antibodies. The immunoprecipitates were eluted and de-crosslinked overnight at 65°C. DNA fragments were extracted, and qPCR was performed for quantification. As negative control, PCR was carried out by using unrelated oligonucleotides, and the presence of equivalent amounts of chromatin in each sample was confirmed by PCR without prior immunoprecipitation (input).

Immunofluorescence and histology

Dissected muscles were snap frozen in liquid nitrogen-cooled isopentane, sectioned (7 µm thick) and stained. For immunofluorescent staining, cells or section were fixed with 4% paraformaldehyde (PFA) and permeabilized in 0.1% Triton X-100, then blocked with 0.5% goat serum and incubated with primary antibody over night at 4°C. After washing out primary antibodies with PBS, cells were incubated with secondary antibodies for one hour at room temperature. Alexa Fluor™ 594, 647 or 488-conjugated secondary antibody was used to detect mouse primary antibodies. Images were acquired with an IX51 Olympus microscope and the Cell*F software or an LSM 980 confocal system (Carl Zeiss). For hematoxylin/eosin staining (H&E), sections were fixed for 15 min and after washes, placed in hematoxylin (Sigma Aldrich, GHS116) for 5 min, and 5 min in eosin (Sigma Aldrich, HT110216). For Oil Red O staining (Sigma-Aldrich, O0625), sections were placed in 60% isopropanol, followed by 75 min

incubation in 0.5 g oil red and 1% of destrin solution in 98% isopropanol; washed in 60% isopropanol then water. The sections were counterstained with Mayer's hematoxylin for 2min. For Sirius Red staining, sections were fixed with 4% PFA for 10 min and stained in Sirius Red solution for 60/90 min at room temperature (RT) protected from light. After washing in acidified water, sections were fixed in 100% ethanol and dehydrated in 100% xylene. Sections were mounted with EUKITT.

Cross sectional area (CSA)

The tibialis anterior (TA) muscles were dissected and fixed in isopentane in liquid nitrogen, and sliced into 7µm sections. The cross-sectional area was analyzed and quantified using CellF*Olympus Imaging Software.

Muscle injury

Animals were anesthetized by a ketaminexylazine cocktail, and 12.5 µl of CTX (60µg/ml *Naja mossambica mossambica*, Sigma-Aldrich, C9759) were injected into and along the length of the right tibialis anterior (TA) (Yan et al., 2003) and 25 µl into gastrocnemius muscle. CTX was injected on different day upon tamoxifen (TAM) treatment.

Transplantation

Freshly isolated MuSCs from Tg:Pax7$^{CreERT2/+}$; D2$^{fl/fl}$; R26^{mTmG} vs Tg:Pax7$^{CreERT2/+}$; D2$^{+/+}$; R26^{mTmG} 12 weeks old TAM- treated mice, were isolated using a FACS machine and were counted, washed with PBS resuspended in PBS with 0.1% BSA at a concentration of 1-3x10^4 cells/20 µl. The receivers 8 weeks old *mdx* mice were anaesthetized by an intraperitoneal injection of a ketaminexylazine cocktail. Donor MuSCs were transplanted into TA receiver *mdx* mice to evaluate skeletal muscle regeneration. The transplantation was performed by slowly injecting 10 µl of the donor cell solution into the TA using a 25µl Hamilton syringe. Each host mouse received transplantation of MuSCs cD2KO into the left TA and MuSCs Ctr into the right TA. Twenty-one and 40 days after transplantation frozen TA muscle sections were processed for immunofluorescence. For transplantation at long time point (40 days post-xenograft), we started to treat mice with tacrolimus (anti-rejection drug) in water at 11 days post xenograft.

Hair follicle cycle

Dorsal back of 3-months-old anesthetized D2KO and control mice were shaved using clamp (Plikus et al., 2008). The mice were harvested after 6 days for the anagen, 10 days for the catagen and 60 days for the telogen analysis and dorsal skin was collected for molecular and histological analysis (Stenn and Paus, 2001).

Wound preparation, macroscopic examination and histological analyses

The back fur of mice was shaved and the skin was cleaned with 70% ethanol. The dorsal skin was pulled using forceps and an 8-mm full-thickness skin wound was created along the midline using a sterile 8 mm

circular biopsy punch by pressing through both layers of the skin pull. Skin wound healing was measured every 2-3 days by anesthetizing the animals and imaging the wounded area. Each wound site was digitally photographed using the Nikon FX-35A camera at the indicated time intervals, and wound areas were examined on photographs using CellF*. Changes in wound areas were expressed as the percentage of the initial wound areas.

EdU incorporation assay *in vivo*

EdU (2.5 mg/ml) was injected in mice contemporary to TAM induction as indicated in figures. EdU was detected using the Click-It kit (Invitrogen, C10337) according to the manufacturer's instructions. Data on EdU incorporation are reported as the percentage of EdU^+ *versus* total cells (measured by DAPI).

Cell size

The cell size of MuSCs was evaluated by analyzing the forward scatter (FSC) by FACS.

Mitochondrial DNA

DNA was extracted from about 50,000 freshly FACS- isolated MuSCs using the QIAamp DNA Micro Kit (Qiagen) according to the manufacturer's instructions. mtDNA was quantified using primers that amplify the cytochrome B region on mtDNA relative to the b-globin region on genomic DNA by RT-qPCR.

Magnetic Sorting of Muscle Stem Cells.

In brief, muscle was dissected from bone in DMEM, minced and digested with 0.1% collagenase A and 0.2% dispase for 30 minutes at 37C°. The collagenase/dispase solution was added to continue the digestion until the process was completely terminated and muscle totally digested. The dissociated single cells were filtered through a 70-micron strainer and pelleted by centrifugation at 400g for 5 mins at 4°C. Cells were washed twice with DMEM and processed with MACS Cell Separation. Muscle stem cells were isolated using the Satellite Cell Isolation Kit (MiltenyiBiotec, 130-104-268). For further purification, muscle stem cells were labeled with Anti-Integrin α-7 MicroBeads (MiltenyiBiotec, 130-104-261) and isolated using LS Columns and a MACS Separator. The flow-through fraction was discarded, and MuSCs were collected in the eluted fraction.

Rosalind™ RNA-seq Methods

Data were analyzed using Rosalind (https://rosalind.onramp.bio/), with a HyperScale architecture developed by OnRampBioInformatics, Inc. (San Diego, CA). Individual sample counts were normalized via Relative Log Expression (RLE) using the DESeq2 R library.

rT3 administration

Mice (C56BL6 mice) were administrated 2 µg/ml of rT3 (Sigma Aldrich #T0281) in drinking water or PBS as control for 10 consecutive days.

Statistical analysis

Significant differences were calculated using ANOVA, and Student's two-tailed t test for independent samples, with p <0.05 considered as statically significant. All statistics and graphics were performed using GraphPad Prism7 and appear in more detail in the SI Appendix, S20. In all figures, error bars represent the SEM. A value of p < 0.05 was considered significant (*P < 0.05; **P < 0.01; ***P < 0.001).

Results

D2 is Expressed in Quiescent Muscle Stem Cells and is Downregulated Upon Cell Activation.

We firstly analysed D2 expression within the different subset of muscle stem cells (Tg:Pax7-nGFP cells) fractionated into distinct subpopulation based on GFP intensity. D2 expression was highest in Pax7-nGFP^{Hi} cells (the most quiescent Pax7 subgroup) (Figure S1A and (Dentice et al., 2014)). Accordingly, in freshly isolated stem cells D2 expression was elevated in quiescent and was dramatically reduced upon proliferation (Figure S1B). Based on these findings, we speculated that D2 could mark quiescent stem cells. To address this issue, we analysed D2 expression by immunofluorescence in the previously characterized 3xFLAG-D2 knock-in mouse (Castagna et al., 2017). We found that D2 co-localized with the muscle stem cell marker Pax7 (Seale et al., 2000) in resting tibialis anterior (TA) muscle (Figure 1A). Interestingly, D2 expression was dynamically regulated in muscle stem cells during lineage progression, where D2 staining co-localized with Pax7^{+} cells at early time points in single isolated muscle fiber, and its expression declined with time (Figure 1B). Accordingly, D2 on fibers was not detectable in proliferating cells identified by 5-ethynyl-2'-deoxyuridine (EdU) incorporation (Figure 1C and 1D), as well as its expression was inversely correlated with D3 (a metabolic marker of proliferative cells (Dentice et al., 2014)) (Figure 1C and 1D). Consistent with the D2-mediated increase of intracellular TH signaling, we observed that other components of the TH signal machinery, namely the *Thra*, *Thrb* receptors, the deiodinase D3 (*Dio3*), the *Mct8*, *Mct10* and *Oatp1c1* transporters were expressed in quiescent muscle stem cells (Figure S1C-l) and appropriately decreased or increased (*Dio3)* as muscle stem cells transited from quiescence to an activation state (Figure S1C-l).

Effects of TH treatment or D2-blocking in MuSCs

Given the expression of D2 in qMuSCs, we asked whether TH-treatment plays a role in stem cells *in vitro*. Freshly isolated FACS sorted MuSCs cultured in 20% FBS plus TH (3 nM T3 and 3 nM T4) for 8 days showed reduced proliferation and S-phase measured by cell counting and Pax7/EdU staining (Figures S2A-D "a" *versus "*b"). Interestingly, cells pre-exposed to TH for 4 days, promptly re-entered the cell cycle upon removal of exogenous TH (Figure S2A, S2C-D, "c" *versus "*b"). Notably, the percentage of Pax7^{+}/EdU^{+} cells decreased and the percent of Pax7^{+}/EdU^{-} cells increased in cells treated with TH only during the last four days (Figures S2A, S2C and S2D, "a" *versus* "d"). In summary, TH treatment delayed proliferation of stem cells while holding them in a reversible G_0 state.

To assess the effects of endogenous D2 in stem cells, we blocked D2 action in cultured myofibers by treating them with rT3 (a specific D2 inhibitor) for 72 hours. Upon D2-blocking, we observed a reduced percentage of quiescent ($Pax7^+/MyoD^-$) cells and an increased percentage of activated ($Pax7^+/MyoD^+$) versus controls (Figure 1E). To assess in greater detail the role of D2 in MuSCs, we genetically ablated D2 in MuSCs by generating Tg:$Pax7^{CreERT2/+}$; $D2^{fl/fl}$ mice (cD2KO) in which TAM treatment induces D2 depletion specifically in MuSCs. Consistent with rT3 treatment, genetic depletion *in vivo* of D2 in cD2KO by TAM treatment before culturing myofibers resulted in a lower percentage of $Pax7^+/MyoD^-$ cells, and a higher percentage of $Pax7^+/MyoD^+$ cells at various time points (Figure 1F). Double staining for Pax7/EdU of single myofibers revealed that the absence of D2 promoted the proliferation of MuSCs (Figure S3A). Accordingly, in myofibers treated with cytosine β-D-arabinofuranoside (ARA, a chemotherapeutic drug that kills cycling cells and spares resting cells), we detected fewer AraC-resistant $Pax7^+$ cells in the absence of D2 versus Ctr (Figure S3B), which suggests that D2-depleted MuSCs are more prone to exit quiescence and proliferate. These results indicate that, upon triggering of cell activation by the isolation procedure, blocking D2 in muscle stem cells boosts their proliferation.

D2 depletion enhances stem cell proliferation during muscle regeneration

To determine the consequences of D2 depletion in MuSCs upon injury, we analysed TA muscles from cD2KO mice collected 21 days after Cardiotoxin (CTX) injection (Figure 2A). D2-depletion resulted in a greater number of centrally nucleated fibers *versus* control, associated with a smaller fibre diameter (Figures 2B-C). Accordingly, the number of $Pax7^+/MyoD^+$ cells, and the equivalent $Pax7^+/BrdU^+$ cells increased while the number of $Pax7^+/MyoD^-$ and the $Pax7^-/MyoD^+$ cells decreased (Figure 2D). This suggested that the absence of D2 increases the proliferative capacity of stem cells while the completion of myogenic program is delayed. This is in agreement with the delayed muscle differentiation we previously observed in global D2 knock-out mice (Dentice et al., 2010). Interestingly, 60 days after CTX injury, fibre diameter was larger in cD2KO mice versus control, which suggests that complete maturation can be achieved in the absence of D2 with prolonged time (Figure 2E).

D2 is required for self-renewal of quiescent MuSCs

When proliferating MuSCs are induced to differentiate by serum deprivation a proportion of them elude terminal differentiation and become “reserve cells” ($Pax7^+/MyoD^-$) (Collins et al., 2005; Yoshida et al., 1998; Zammit et al., 2004). The reduction in number of quiescent cells upon D2-depletion ($Pax7^+/MyoD^-$, Fig. 2D) prompted us to investigate whether D2 plays a role in the capacity of stem cells to constitute the “reserve population”. In other words, we analysed whether activated MuSCs can re-enter quiescence in the absence of D2. Upon induced differentiation, we observed a reduced capacity to generate “reserve cells” ($Pax7^+/MyoD^-$) in the absence of D2 (Figure 2F-G). Accordingly, when we exposed MuSCs to serum deprivation and rT3, the number of $Pax7^+/MyoD^-$ reserve cells was lower than that of control (Figure S3C), which supports the concept that D2 is required to re-enter quiescence. Of note, D2-depletion was associated with increased number of activated cells ($Pax7^+/MyoD^+$) (Figure 2G) and a reduced myogenic

differentiation (Desmin and MyHC2) (Figure 2H) which is in agreement with the role in promoting terminal differentiation subsequently played by a second surge in D2 during the differentiation program (Dentice et al., 2010).

To evaluate whether the reduced number of quiescent ($Pax7^+/MyoD^-$) cells upon injury (Figure 2D) reflects the inability to restore the stem cell reservoir in the absence of D2, we investigated whether D2-depleted stem cells could normally re-constitute the stem cell pool *in vivo*. To this aim, we analysed muscle repair after five consecutive CTX injuries at 30 days after the last CTX (Figure 2I). In this setting, the number of quiescent MuSCs ($Pax7^+/MyoD^-$) was lower in cD2KO mice (Figure 2J). Furthermore, in D2-depleted muscles after multiple injuries, areas of non-muscle tissue were larger than control (Figure 2K-L), while the diameter of the newly formed muscle fibers was reduced (Figure 2M). Accordingly, we found increased intramuscular fibrosis, which confirms MuSCs failure in cD2KO upon consecutive damages (Figures 2N-O). Overall, these data indicate a self-renewal deficiency of D2-depleted stem cells that leads to a gradual depletion of resident stem cells and consequent increased fibrosis after muscle injuries. Accordingly, by using a different mouse model (Tg:$Pax7^{CreERT2/+}$; $R26^{mTmG}$; $D2^{fl/fl}$ versus Tg:$Pax7^{CreERT2/+}$; $R26^{mTmG}$; $D2^{+/+}$), in which green epifluorescence labels newly generated D2-depleted fibers, we observed that newly generated D2-depleted green fibres were fewer but larger in absence of D2 versus control after three consecutive CTX injuries (Figures S4A-C). Moreover, *Pax7* and *MyHC2* mRNA levels were lower in triple injured cD2KO muscle than in control (Figure S4D). These results suggest that after multiple injuries MuSCs fail to repopulate the stem cell reservoir in cD2KO mice.

D2-derived TH sustains the Notch pathway

To shed light on the molecular mechanisms triggered by D2 depletion in quiescent stem cells, we purified MuSCs by magnetic separation from cD2KO *versus* control mice in resting muscle and analysed the cell transcriptome by RNA-sequencing analysis immediately thereafter. About thirteen hundred genes were significantly altered in cD2KO MuSCs *versus* controls, of which approximately half were downregulated and half were upregulated (Figure 3A). Functional analysis identified multiple pathways affected by D2-depletion (Fig. 3B-C); among the pathways downregulated by D2-depletion, the Notch signaling pathway stands out as a potential regulator of stemness (Figure 3B).

We validated this finding in FACS isolated Pax-$nGFP^+$ cells, and found that relevant Notch targets (*HeyL, Hes2 and Rbpj*) and Notch receptors (*Notch1, Notch2, Notch3 and Notch4*) were downregulated at the mRNA level in cD2KO MuSCs (Figure 3D). Importantly, Western blot revealed lower levels of the active Notch Intracellular protein (NICD) in D2-depleted cells (Figure 3E). We next evaluated whether the TH nuclear receptor directly binds Notch receptor loci. In silico analysis revealed the presence of multiple putative TH-responsive-elements (TRE) in the locus of two Notch receptors, i.e. Notch2 and Notch3 (Figure 3F). Chromatin Immunoprecipitation (ChIP) assay confirmed the binding of TH receptor (TR) to one site of Notch2 and one site of Notch3 (3 and 38-fold enrichment respectively in the presence of TR antibody; Figure 3G). These experiments suggest that, in MuSCs D2 is an upstream regulator of Notch, that acts via a direct TRα-mediated transcriptional regulation of the Notch receptors 2 and 3. To assess

whether active Notch could functionally rescue D2 depletion *in vivo*, we generated $Pax7^{CreERT2/+}$; $D2^{fl/fl}$; $R26^{stop-NICD-nGFP}$ (hereafter referred to as cD2KO-N1ICD) mice in which D2 was excised in MuSCs with simultaneous Notch over-activation. We characterized the MuSC population in regenerating TA muscles at 7 (Figure S5) and 21 (Figure 3H) days after CTX of cD2KO/N1ICD and cD2KO mice. Immunofluorescence staining showed a reduction of the percentage of $Pax7^+/EdU^+$ cells (as well as of $Pax7^+/MyoD^+$ cells) and a corresponding increase in $Pax7^+/EdU^-$ cells in cD2KO/N1ICD mice *versus* control (Figures 3I and 3J), which indicates that the effects of D2 depletion was substantially rescued by Notch overexpression. These data show that D2 is required to sustain Notch signaling in quiescent stem cells, and that forced Notch activity can rescue some of the effects of D2 depletion.

D2 regulates the entry of quiescent MuSCs cells into a G_{Alert} state in resting muscle

Quiescent MuSCs can cycle between two molecular states: a dormant (G_0) state and a primed but still non-dividing state (G_{Alert}) induced in response to generalized tissue injury. The G_{Alert} phase is characterized by an increased cell size and mitochondrial DNA, a rapid entry into the cell cycle, and a dependency on the mammalian target-of-rapamycin (mTORC1) (Rodgers et al., 2014). In MuSC isolated from resting muscles, “Cell cycle” was among the upregulated pathways induced as a consequence of D2 depletion (Figure 3C). In resting conditions FACS counting of $Edu^+/Pax7\text{-}nGFP^+$ cells revealed that the number of D2-depleted cells exceeded that of controls, and moreover that it reached a percentage level comparable to the wild type “Alerted cells” (Figure 4A). However, D2 depletion alone was unable to fully activate cell proliferation as induced by injury (Figure 4A). To assess whether D2-depletion in MuSCs is able by itself to “alert” cells, we measured known markers of the G_{Alert} state in resting muscle. This experiment showed that D2-depletion activates mTORC1 as witnessed by increased levels of phospho-mTOR (Figure 4C), as well as its target phospho-S6-ribosomal protein (Figure 4D) and phospho-S6K (Figure 4E). Activation of the mTOR pathway could depend on the reduction of AMPK activity, which in turn regulates mTOR. Interestingly p-AMPK was potently downregulated by D2-depletion (Figure 4F), which suggests a mechanism by which D2-depletion increases mTORC1 by attenuating AMPK activity. We also found that D2-depleted MuSCs have increased mitochondrial DNA content (Figure 4G) and are larger than Ctr as measured by FACS (Figure 4H). Thus, these findings indicated that D2-depletion can induce an “Alert state” in MuSCs.

In parallel, we also evaluated whether a change in D2 levels also occurs in “alerted” MuSCs. Interestingly, D2 was drastically lower in G_{Alert} cells than in quiescent G_0 cells (Figure 4I), which is consonant with the role that D2 plays in the “alerting” process. Lastly, we compared in silico the genes differentially expressed in cD2KO versus control MuSCs (Fig. 3A) with those induced in the G_{Alert} state deposited in the GSE55490 database (Rodgers et al., 2014). Interestingly, of the 678 down-regulated genes in cD2KO, 52 overlap with the down-regulated genes in G_{Alert} state ($p < 2.418^{e-16}$); while of the 611 up-regulated genes in cD2KO, 26 overlap with the up-regulated genes in a G_{Alert} state ($p < 0.041$) (Figure 4J-K). Overall, these data indicate that D2 depletion causes a condition whose transcriptionally signature significantly

overlaps with the G_{Alert} state and support the finding that D2-depletion is sufficient alone to cause an “Alerted state” in muscle stem cells.

To test the effects of chronic D2 depletion in resting muscles, we compared Tg:Pax7$^{CreERT2/+}$; R26^{mTmG}; D2$^{fl/fl}$ with Tg:Pax7$^{CreERT2/+}$; R26^{mTmG}; D2$^{+/+}$ 4 months upon D2-depletion (Figure S6). Under these conditions, we observed that the D2-depleted fibres (green ones) were more numerous (Figures S6A-B) and their diameters were smaller compared to controls (Figure S6C). Taken together, these findings suggest that quiescent MuSCs can transit from a G_0 to a G_{Alert} state upon D2-depletion. In the long term, the combination of the Alert state and the physiological muscle turnover stimuli determines an increased number of newly generated fibres in D2-depleted versus control muscles.

Characterization of the Phenotype of the mdx-D2KO Mice and Transplantation Assays to Evaluate Cell Engrafting Potential In Vivo After D2-depletion

Premature exhaustion of muscle stem cells is a major determinant of the dystrophic process (Bianchi et al., 2020; Ontell, 1986). We asked whether D2-depletion could affect the dystrophic phenotype of *mdx* mice. To this aim, we generated *mdx*/global-D2 knock-out (*mdx*-D2KO) mice and characterized the muscle phenotype using morphological and molecular analyses. We measured Pax7 and neo-MHC mRNA levels in a period from 4 to 50 weeks postnatally, and found that both markers were higher in *mdx*-D2KO mice than in controls (Figure 5A). Increased number of Pax7^{+} cells were also detected in TA muscle in *mdx*-D2KO mice vs *mdx* mice (at 4 weeks post-natal, which is the peak of dystrophy) (Figure 5B). At 4 weeks, while fiber size in *mdx*-D2KO mice was smaller, the number of fibers was increased (Figures 5C-E). In addition, the levels of myogenin and MyoD were higher, whereas the levels of Creatine Kinase (CK) lower in *mdx*-D2KO mice versus control (Figure 5F). Thus, global D2-depletion in the *mdx* context results in a delayed dystrophic phenotype, a significantly increased number of muscle stem cells associated with a more temporally sustained regenerative potential.

Based on the data obtained with the *mdx*-D2KO mice, we tested the functional capability of D2-depleted MuSCs to engraft *in vivo* by conducting a transplantation assay. We isolated MuSCs from donor Tg:Pax7$^{CreERT2/+}$; R26^{mTmG}; D2$^{fl/fl}$ versus Tg:Pax7$^{CreERT2/+}$; R26^{mTmG}; D2$^{+/+}$ mice and injected these into the TA of *mdx* mice (Figure 5G). Engraftment of donor-derived myofibers in *mdx* recipients was analysed by direct epifluorescence for green fluorescent protein on TA muscle harvested 21 and 40 days after transplantation (Figure 5H). The number of GFP-positive D2-depleted fibres was increased at both 21 and 40 days after transplantation (Figure 5I), which is in agreement with the enhanced proliferation rate of D2-depleted cells. Cross sectional area (CSA) analysis showed that- D2-depleted fibres were smaller at 21 days and larger at 40 days versus control, which indicates that D2-deficiency could be compensated at a later time (Figure 5J), which is in agreement with D2-depletion *in vivo* (Fig. 2B and Fig. 2E).

Overall, there results indicate that D2-depleted MuSCs successfully engraft, have an increased proliferative capacity and a time-dependent delay in maturation that is compensated at later time points.

D2-depletion affects stem cell homeostasis in skin

To assess whether D2 expression in stem cells is limited to muscle or is a common feature shared by other tissues, we analyzed the localization of D2 in skin. Interestingly, D2 expression co-localized with the hair follicle stem-cell marker CD34, which specifically marks the bulge region of the hair follicle, which is where quiescent stem cells are localized (Figure 6A). In addition, we found that D2 expression was dynamically regulated during the hair follicle cycle. In fact, D2 was clearly detectable in the telogen phase, the resting phase of the hair follicle cycle, and never coincided with EdU labelling (Figure 6B).

To investigate the role of D2 in the hair follicle stem cells we generated a skin conditional D2KO (scD2KO) mouse model (Tg:K14$^{CreER/+}$; D2$^{fl/fl}$). Interestingly, the percentage of CD34^{+}/alpha 6 integrin^{+} cells (hair follicle stem cell markers), significantly increased 6 days upon D2-depletion (Figure 6C). These results indicate that, similar to what we observed in muscle, blocking D2 in hair follicle stem cells, promotes their proliferation.

Next, we analysed the effects of specific D2-depletion in the hair follicle compartment of mice subjected to one (T1) or three (T3) consecutive rounds of hair depilation. We observed that the number of Sox9^{+}/EdU^{+} cells in the hair follicle bulges increased upon D2-depletion after a single round of depilation (T1), while three rounds of depilation caused a net decrease in EdU^{+} and Sox9^{+} cells (Figure 6D). Accordingly, Sox9 and CD34 mRNAs were initially increased at T1, and reduced at T3 (Figures 6E), thus suggesting that while D2 depletion initially increased the activation of stem cells, it caused cell exhaustion following subsequent rounds of amplification. To characterize the effects of D2-depletion *in vivo* during tissue regeneration, we performed a wound healing assay. The time course of regenerating epidermis showed that the closure of the wound was significantly faster in D2-depleted epidermis than in control skin (Figure 6F). Overall, these data indicate that D2 plays a key role in preserving hair follicle stem cells from uncontrolled activation.

Drug-induced D2-inhibition as novel therapeutic tool to enhance expansion of activated precursor cells.

To therapeutically exploit the capacity of D2-depletion to alert stem cells and accelerate muscle tissue repair, we treated mice with oral rT3 (a specific D2-inhibitor) for 7 days (-5/+2 relative to CTX injury) (Figure 7A). Hematoxylin & Eosin (H&E) analysis 7 days post-CTX revealed more fibers in rT3- treated than in controls mice (Figures 7B and C). In rT3-treated mice, Pax7^{+}/EdU^{+} cells were increased and fibers were smaller than in control mice (Figure 7D). Importantly, 21 days after injury we observed larger fibers in rT3 treated mice than control, which is in agreement with the limited time frame (7 days) of D2 inhibition (Figures 7E and F). In a similar setting, we tested whether D2 inhibition positively affected wound regeneration in skin, and found that rT3-treated mice repair wounds more rapidly and efficiently than control mice (Figures 7G). In summary, we demonstrate that drug-induced D2-blocking with rT3 facilitates regeneration, -likely alerting stem cells-, in different tissue contexts and could be therapeutically exploited *in vivo*.

Discussion

Cellular quiescence is a property of several adult vertebrate stem cells. How this condition is regulated and preserved is a central issue in stem cell biology which still remains poorly understood.

Here we report that D2 is a key metabolic enzyme that acts as a master regulator of muscle stem cell quiescence. The D2 -mediated action represents a functional link between the circulating thyroid hormone concentrations and a cell-autonomous mechanism that enables to customize intracellular TH and preserve quiescence and stem cell function.

The temporal expression pattern of D2 is peculiar. Indeed, *Dio2* mRNA is elevated in quiescence, drastically reduced upon activation and back on at a later phase of myogenesis to allow full differentiation (Figure S1B). This peculiar D2 expression is consistent with previously reported mRNA data set in quiescent vs activated muscle stem cells (GSE47177 (Liu et al., 2013), Fig. S1J). Our data also indicate that in activated stem cells D2 is re-expressed in a subset of cells and that this process is relevant for the return to quiescence and, moreover is required to restore the normal stem cell reservoir under normal conditions (Fig. 2F-H). In the absence of D2, proliferating myoblasts fail to self-renew and this would eventually cause depletion of the stem cell pool (Fig. 2I-O and S4).

The role of D2 in quiescence is unknown. We propose that D2 acts as a sensor/effector rheostat of the normal environment by increasing intracellular TH concentrations in stem cells to preserve the quiescence state. Thyroid hormone acts as a pro-differentiating agent in several cell contexts (Dentice et al., 2010; Garcia-Serrano et al., 2011) and, the increased TH concentration we found in stem cells is likely a mechanism to defend quiescence from undesired breaking signals present in the microenvironment. In this setting, D2-produced TH acts as a cell autonomous signal that sustains stem cell quiescence. Upon disruption of the niche, D2 is sharply downregulated in stem cells thereby allowing them to exit quiescence. The signals regulating D2 expression in quiescent cells are presently unknown and represent the aim of future studies. While it is well known from clinical observations in patients with thyroid dysfunction that TH influences tissue homeostasis and regeneration, the underlying mechanisms are obscure. The identification of the D2 specifically expressed in the quiescent stem cell compartment in both muscle and skin added TH signaling to the list of key players in the mechanisms controlling quiescence, tissue homeostasis and regeneration.

D2 is, to our knowledge, the only TH-related protein known to keep and preserve quiescence in solid organ stem cells. Our data indicate that the D2 gene program affects the stem cell niche in the skeletal muscle as well as in such other tissues as skin (Figure 6) and brain (data not shown) which also specifically express D2 in the stem cell compartment. What are the molecular mechanisms by which D2 controls quiescence? Our RNA-seq analysis of quiescent MuSCs cells isolated from cD2KO vs control revealed that Notch signaling is down-regulated at multiple levels upon D2 genetic depletion (Figure 3B). The Notch pathway is a key regulator of many types of adult stem cells, and its activity has been shown to be instrumental for the regulation of cell fates and proliferation in a variety of tissues. Quiescent MuSCs are characterized by elevated Notch activity that is required for their maintenance. By Chromatin

immunoprecipitation, we demonstrated that the TH receptor alpha directly binds to the Notch2 and Notch3 gene loci and promotes their expression (Figure 3G). The functional association between Notch and D2 was first observed in a study of the expression profile of Pax7-nGFP sub-sorted cells wherein both D2 and Notch activity reached their highest level in the GFP^{high} subpopulation- (Figure S1 and (Dentice et al., 2014). Using different combinations of genetically modified mice with altered D2 and Notch levels, we found D2 epistatically located upstream of Notch in quiescent MuSCs. Notch signaling is necessary and sufficient to preserve quiescence and could rescue the phenotype observed upon D2 depletion. In fact, imposed contemporary expression of active Notch substantially rescued the phenotype of D2-depletion *in vivo* (Figure 3H-I and S5). However, we measured Notch-mediated rescue by analyzing only a few markers (Figure 3H-I and S5) and given the pleiotropic effects of TH it is likely that other genes/pathways are regulated by TH and influence MuSCs behavior which are not compensated by Notch overexpression. Of note, the role of Notch signaling in actively promoting self-renewal of muscle stem cells through direct regulation of Pax7 is also consistent with the reduced self-renewal observed in cD2KO cells, thereby sustaining the idea of a large overlapping and upstream position of TH respect to Notch signaling. In any case, our studies specifically identified Notch signaling to be a principal mediator of TH in controlling the quiescent state, which illustrate a novel mechanism TH-dependent of muscle stem cell control of quiescence.

What are the consequences of D2 depletion? We found that, in resting condition, MuSCs specific D2-depletion induces the transition from G_0 to G_{Alert} while it promotes cell proliferation and expansion in regenerative conditions. Reducing TH induces a break in quiescence and a transition into a G_{Alert} state. The sustained D2-mediated TH action is then responsible for the maintenance of quiescence in resting muscle. The transition from G_0 to G_{Alert} was initially demonstrated in quiescent cells by the action of systemic HGFA released upon muscle injury (Rodgers et al., 2017). Here we found that a metabolic decrease in TH intracellular concentration by D2 depletion alone is sufficient to induce G_{Alert} without any other systemic cues. Mechanistically, we found that, D2 depletion activates mTOR and S6K and causes a corresponding reduction in pAMPK (Figure 4C-F). The effects of D2-depletion and corresponding reduction of TH concentration are in agreement with the previously reported effects of TH treatment on stimulating pAMPK levels in C2C12 myoblasts (Yamauchi et al., 2008). In this scenario, it is reasonable to hypothesize that the well-known capacity of TH to induce rapid mobilization of intracellular Ca+ levels (Irrcher et al., 2008; Yamauchi et al., 2008) could act as a molecular trigger of CAMKK activity and then pAMPK/mTORC.

Interestingly, the molecular gene program triggered by D2-depletion is significantly coincident with the gene signature triggered by the Alert condition (Figure 4J-K), which strongly supports the notion that a large overlapping exists between D2-depletion and the transition into G_{Alert}.

Of note, the mechanisms that cause, by systemic cues, entry into G_{Alert} also determine a reduction of D2 levels. The reduced D2 expression level measured in systemically Alerted MuSCs (Figure 4I) represented an important support to the association between G_{Alert} and D2 action. The molecular mechanisms for

that are presently unknow, but it is not inconceivable to hypothesize a potential inhibition of D2 levels by circulating growth factors (e.g. HGFA) normally acting as alarmins in the plasma. Our study demonstrates that a complex metabolic pathway that defines T3 concentration in the intracellular milieu controls the transition from G_0 into G_{Alert}.

In regenerative conditions, D2-depletion increases the number of proliferating myoblasts thereby favoring progenitors expansion. However, “reserve experiments” also indicate that D2 action is required in order to return proliferating precursor myoblasts to quiescence (Figure 2F-H and S4). *In vivo*, this translates into a functional deficiency to restore the stem cell reservoir in the event of multiple challenges as observed in muscle (Figure 2J) and skin (Figure 6E). While we previously demonstrated that in global D2KO mice sustained MuSCs proliferation is associated with delayed differentiation and muscle repair, our temporally transient pharmacological block of D2-action, induced by rT3 treatment *in vivo*, indicates that we could favor expansion of stem cells at an early stage of regeneration/wound healing without hampering the subsequent differentiation capacity (Figure 7), which ultimately leads to faster repair of injured muscle and skin. Vice versa, permanent D2-depletion has negative consequences due to reduced self-renewal coupled to a delayed differentiation (Figure S4).

The capacity of D2-depletion to enhance cell proliferation was confirmed by the engrafting experiments, which showed enhanced engrafting potential of D2-depleted cells vs control. The reduced exhaustion of the stem cell pool was confirmed also by the delayed onset of dystrophic phenotype observed in mdx-D2KO mice. This is likely the result of a potentiated expansion of muscle stem cells which– in absence of D2- determine a larger pool of progenitor myoblasts in mdx-D2KO mice that eventually, with a time delay-differentiate into myotubes. The increased expansion of activated myoblasts pool is likely the explanation for the positive effects observed upon D2-blocking in stem cells in acute regenerative conditions (i.e. in muscle injury and wound healing) as well as in the mdx-D2KO context, where the onset of dystrophy is delayed and the number of Pax7 cells is retained with time respect to control. This result suggests that D2 -depletion is beneficial for the expansion of the progenitor cell pool in both normal and pathological settings.

The quiescence-sustaining function of D2 in skeletal muscle is likewise distinct from its effect in other tissues such as the heart, where it can act to induce cardiomyocyte proliferation (Li et al., 2014) or in cancer cells where it acts as a regulator of cancer progression and metastasis formation (Miro et al., 2019). While we report that D2 action affects the muscle niche via the Notch pathway, it would be of interest to investigate whether the TH-Notch signaling cascade we report applies to stem cell compartments in other tissues and organisms.

Lastly, the regulatory mechanism we describe provides a framework to construct a more dynamic view of the stem cell niche, and pave the way to exploit a signal derived from a soluble hormone to manipulate stem cell behavior in a therapeutic context. The pharmacological blocking of D2-action by rT3 treatment *in vivo* provides a proof-of-principle for the therapeutic exploitation of these results. In this scenario, we demonstrate an increase in the number of fibers and activated myoblasts in rT3 treated mice (Figures 7B

and 7C), which repair wounds more rapidly and efficiently than control animals. Overall, this study identifies TH-dependent signaling as intracellular metabolic hub that is responsible for the maintenance of quiescence. It establishes a direct connection between a hormonal signal and the control of quiescence in solid organ stem cells and that also illustrates their potential use in stem cell-based therapies.

Abbreviations

Muscle Stem cells (MuSCs); quiescent Muscle Stem Cells (qMuSCs); stem cells (SCs); Thyroid Hormone (TH); Type 2 deiodinase (D2); Type 3 deiodinase (D3).

Declarations

ACKNOWLEDGMENTS

This research was funded by the grant from the European Research Council under the European Union's Horizon2020 Programme—EU FP7 contract Thyrage (grant number 666869) and by the grant AFM-Telethon (grant number 23276) to D.S. We thank Jean Ann Gilder (Scientific Communication srl., Naples, Italy) for editing the text.

AUTHOR CONTRIBUTIONS. M.A.D.S., R.A., C.L., G.M., D.D.G. performed *in vitro* and *in vivo* experiments and prepared figures. Conceptualization, D.S.; Formal Analysis, M.A.D.S.; R.A.; C.L.; D.D.G.; M.D.; G.M.; F.V.; E.D.C. and C. Miro.; Investigation, M.A.D.S.; Observations and scientific interpretations, C. Missero; Writing, M.A.D.S. and D.S.; Supervision, D.S.

DECLARATION OF INTERESTS. The authors declare no competing interests

The authors have declared no conflict of interest.

References

Ambrosio, R., De Stefano, M.A., Di Girolamo, D., and Salvatore, D. (2017). Thyroid hormone signaling and deiodinase actions in muscle stem/progenitor cells. Molecular and cellular endocrinology *459*, 79-83.

Anderson, J.E., Liu, L., Kardami, E., and Murphy, L.J. (1994). The pituitary-muscle axis in mdx dystrophic mice. Journal of the neurological sciences *123*, 80-87.

Baghdadi, M.B., Firmino, J., Soni, K., Evano, B., Di Girolamo, D., Mourikis, P., Castel, D., and Tajbakhsh, S. (2018). Notch-Induced miR-708 Antagonizes Satellite Cell Migration and Maintains Quiescence. Cell stem cell *23*, 859-868 e855.

Bianchi, A., Mozzetta, C., Pegoli, G., Lucini, F., Valsoni, S., Rosti, V., Petrini, C., Cortesi, A., Gregoretti, F., Antonelli, L.*, et al.* (2020). Dysfunctional polycomb transcriptional repression contributes to lamin A/C-

dependent muscular dystrophy. The Journal of clinical investigation *130*, 2408-2421.

Bianco, A.C., Dumitrescu, A., Gereben, B., Ribeiro, M.O., Fonseca, T.L., Fernandes, G.W., and Bocco, B. (2019). Paradigms of Dynamic Control of Thyroid Hormone Signaling. Endocrine reviews *40*, 1000-1047.

Bjornson, C.R., Cheung, T.H., Liu, L., Tripathi, P.V., Steeper, K.M., and Rando, T.A. (2012). Notch signaling is necessary to maintain quiescence in adult muscle stem cells. Stem cells *30*, 232-242.

Bodo, E., van Beek, N., Naumann, V., Ohnemus, U., Brzoska, T., Abels, C., and Paus, R. (2009). Modulation of chemotherapy-induced human hair follicle damage by 17-beta estradiol and prednisolone: potential stimulators of normal hair regrowth by "dystrophic catagen" promotion? The Journal of investigative dermatology *129*, 506-509.

Brack, A.S., and Rando, T.A. (2012). Tissue-specific stem cells: lessons from the skeletal muscle satellite cell. Cell stem cell *10*, 504-514.

Castagna, M.G., Dentice, M., Cantara, S., Ambrosio, R., Maino, F., Porcelli, T., Marzocchi, C., Garbi, C., Pacini, F., and Salvatore, D. (2017). DIO2 Thr92Ala Reduces Deiodinase-2 Activity and Serum-T3 Levels in Thyroid-Deficient Patients. The Journal of clinical endocrinology and metabolism *102*, 1623-1630.

Christoffolete, M.A., Arrojo e Drigo, R., Gazoni, F., Tente, S.M., Goncalves, V., Amorim, B.S., Larsen, P.R., Bianco, A.C., and Zavacki, A.M. (2007). Mice with impaired extrathyroidal thyroxine to 3,5,3'-triiodothyronine conversion maintain normal serum 3,5,3'-triiodothyronine concentrations. Endocrinology *148*, 954-960.

Collins, C.A., Olsen, I., Zammit, P.S., Heslop, L., Petrie, A., Partridge, T.A., and Morgan, J.E. (2005). Stem cell function, self-renewal, and behavioral heterogeneity of cells from the adult muscle satellite cell niche. Cell *122*, 289-301.

Contreras-Jurado, C., Garcia-Serrano, L., Martinez-Fernandez, M., Ruiz-Llorente, L., Paramio, J.M., and Aranda, A. (2014). Impaired hair growth and wound healing in mice lacking thyroid hormone receptors. PloS one *9*, e108137.

Dentice, M., Ambrosio, R., Damiano, V., Sibilio, A., Luongo, C., Guardiola, O., Yennek, S., Zordan, P., Minchiotti, G., Colao, A.*, et al.* (2014). Intracellular inactivation of thyroid hormone is a survival mechanism for muscle stem cell proliferation and lineage progression. Cell metabolism *20*, 1038-1048.

Dentice, M., Luongo, C., Huang, S., Ambrosio, R., Elefante, A., Mirebeau-Prunier, D., Zavacki, A.M., Fenzi, G., Grachtchouk, M., Hutchin, M.*, et al.* (2007). Sonic hedgehog-induced type 3 deiodinase blocks thyroid hormone action enhancing proliferation of normal and malignant keratinocytes. Proceedings of the National Academy of Sciences of the United States of America *104*, 14466-14471.

Dentice, M., Marsili, A., Ambrosio, R., Guardiola, O., Sibilio, A., Paik, J.H., Minchiotti, G., DePinho, R.A., Fenzi, G., Larsen, P.R.*, et al.* (2010). The FoxO3/type 2 deiodinase pathway is required for normal mouse

myogenesis and muscle regeneration. The Journal of clinical investigation *120*, 4021-4030.

Feige, P., Brun, C.E., Ritso, M., and Rudnicki, M.A. (2018). Orienting Muscle Stem Cells for Regeneration in Homeostasis, Aging, and Disease. Cell stem cell *23*, 653-664.

Fuchs, E., and Blau, H.M. (2020). Tissue Stem Cells: Architects of Their Niches. Cell stem cell *27*, 532-556.

Fuchs, E., Tumbar, T., and Guasch, G. (2004). Socializing with the neighbors: stem cells and their niche. Cell *116*, 769-778.

Fujimaki, S., Seko, D., Kitajima, Y., Yoshioka, K., Tsuchiya, Y., Masuda, S., and Ono, Y. (2018). Notch1 and Notch2 Coordinately Regulate Stem Cell Function in the Quiescent and Activated States of Muscle Satellite Cells. Stem cells *36*, 278-285.

Garcia-Serrano, L., Gomez-Ferreria, M.A., Contreras-Jurado, C., Segrelles, C., Paramio, J.M., and Aranda, A. (2011). The thyroid hormone receptors modulate the skin response to retinoids. PloS one *6*, e23825.

Gereben, B., Zavacki, A.M., Ribich, S., Kim, B.W., Huang, S.A., Simonides, W.S., Zeold, A., and Bianco, A.C. (2008). Cellular and molecular basis of deiodinase-regulated thyroid hormone signaling. Endocrine reviews *29*, 898-938.

Irrcher, I., Walkinshaw, D.R., Sheehan, T.E., and Hood, D.A. (2008). Thyroid hormone (T3) rapidly activates p38 and AMPK in skeletal muscle in vivo. Journal of applied physiology *104*, 178-185.

Li, M., Iismaa, S.E., Naqvi, N., Nicks, A., Husain, A., and Graham, R.M. (2014). Thyroid hormone action in postnatal heart development. Stem cell research *13*, 582-591.

Liu, L., Cheung, T.H., Charville, G.W., Hurgo, B.M., Leavitt, T., Shih, J., Brunet, A., and Rando, T.A. (2013). Chromatin modifications as determinants of muscle stem cell quiescence and chronological aging. Cell reports *4*, 189-204.

Luongo, C., Dentice, M., and Salvatore, D. (2019). Deiodinases and their intricate role in thyroid hormone homeostasis. Nature reviews Endocrinology *15*, 479-488.

Luongo, C., Martin, C., Vella, K., Marsili, A., Ambrosio, R., Dentice, M., Harney, J.W., Salvatore, D., Zavacki, A.M., and Larsen, P.R. (2015). The selective loss of the type 2 iodothyronine deiodinase in mouse thyrotrophs increases basal TSH but blunts the thyrotropin response to hypothyroidism. Endocrinology *156*, 745-754.

Miro, C., Di Cicco, E., Ambrosio, R., Mancino, G., Di Girolamo, D., Cicatiello, A.G., Sagliocchi, S., Nappi, A., De Stefano, M.A., Luongo, C.*, et al.* (2019). Thyroid hormone induces progression and invasiveness of squamous cell carcinomas by promoting a ZEB-1/E-cadherin switch. Nature communications *10*, 5410.

Mourikis, P., Sambasivan, R., Castel, D., Rocheteau, P., Bizzarro, V., and Tajbakhsh, S. (2012). A critical requirement for notch signaling in maintenance of the quiescent skeletal muscle stem cell state. Stem cells *30*, 243-252.

Ontell, M. (1986). Muscular dystrophy and muscle regeneration. Human pathology *17*, 673-682.

Paus, R. (2010). Exploring the "thyroid-skin connection": concepts, questions, and clinical relevance. The Journal of investigative dermatology *130*, 7-10.

Plikus, M.V., Mayer, J.A., de la Cruz, D., Baker, R.E., Maini, P.K., Maxson, R., and Chuong, C.M. (2008). Cyclic dermal BMP signalling regulates stem cell activation during hair regeneration. Nature *451*, 340-344.

Rocheteau, P., Gayraud-Morel, B., Siegl-Cachedenier, I., Blasco, M.A., and Tajbakhsh, S. (2012). A subpopulation of adult skeletal muscle stem cells retains all template DNA strands after cell division. Cell *148*, 112-125.

Rodgers, J.T., King, K.Y., Brett, J.O., Cromie, M.J., Charville, G.W., Maguire, K.K., Brunson, C., Mastey, N., Liu, L., Tsai, C.R.*, et al.* (2014). mTORC1 controls the adaptive transition of quiescent stem cells from G0 to G(Alert). Nature *510*, 393-396.

Rodgers, J.T., Schroeder, M.D., Ma, C., and Rando, T.A. (2017). HGFA Is an Injury-Regulated Systemic Factor that Induces the Transition of Stem Cells into GAlert. Cell reports *19*, 479-486.

Rudnicki, M.A., Le Grand, F., McKinnell, I., and Kuang, S. (2008). The molecular regulation of muscle stem cell function. Cold Spring Harbor symposia on quantitative biology *73*, 323-331.

Safer, J.D., Crawford, T.M., and Holick, M.F. (2005). Topical thyroid hormone accelerates wound healing in mice. Endocrinology *146*, 4425-4430.

Safer, J.D., Fraser, L.M., Ray, S., and Holick, M.F. (2001). Topical triiodothyronine stimulates epidermal proliferation, dermal thickening, and hair growth in mice and rats. Thyroid : official journal of the American Thyroid Association *11*, 717-724.

Seale, P., Sabourin, L.A., Girgis-Gabardo, A., Mansouri, A., Gruss, P., and Rudnicki, M.A. (2000). Pax7 is required for the specification of myogenic satellite cells. Cell *102*, 777-786.

Slominski, A., and Wortsman, J. (2000). Neuroendocrinology of the skin. Endocrine reviews *21*, 457-487.

Slominski, A., Wortsman, J., Kohn, L., Ain, K.B., Venkataraman, G.M., Pisarchik, A., Chung, J.H., Giuliani, C., Thornton, M., Slugocki, G.*, et al.* (2002). Expression of hypothalamic-pituitary-thyroid axis related genes in the human skin. The Journal of investigative dermatology *119*, 1449-1455.

Stenn, K.S., and Paus, R. (2001). Controls of hair follicle cycling. Physiological reviews *81*, 449-494.

Tumbar, T., Guasch, G., Greco, V., Blanpain, C., Lowry, W.E., Rendl, M., and Fuchs, E. (2004). Defining the epithelial stem cell niche in skin. Science *303*, 359-363.

van Beek, N., Bodo, E., Kromminga, A., Gaspar, E., Meyer, K., Zmijewski, M.A., Slominski, A., Wenzel, B.E., and Paus, R. (2008). Thyroid hormones directly alter human hair follicle functions: anagen prolongation and stimulation of both hair matrix keratinocyte proliferation and hair pigmentation. The Journal of clinical endocrinology and metabolism *93*, 4381-4388.

Wang, Y.X., and Rudnicki, M.A. (2011). Satellite cells, the engines of muscle repair. Nature reviews Molecular cell biology *13*, 127-133.

Wen, Y., Bi, P., Liu, W., Asakura, A., Keller, C., and Kuang, S. (2012). Constitutive Notch activation upregulates Pax7 and promotes the self-renewal of skeletal muscle satellite cells. Molecular and cellular biology *32*, 2300-2311.

Yamauchi, M., Kambe, F., Cao, X., Lu, X., Kozaki, Y., Oiso, Y., and Seo, H. (2008). Thyroid hormone activates adenosine 5'-monophosphate-activated protein kinase via intracellular calcium mobilization and activation of calcium/calmodulin-dependent protein kinase kinase-beta. Molecular endocrinology *22*, 893-903.

Yan, Z., Choi, S., Liu, X., Zhang, M., Schageman, J.J., Lee, S.Y., Hart, R., Lin, L., Thurmond, F.A., and Williams, R.S. (2003). Highly coordinated gene regulation in mouse skeletal muscle regeneration. The Journal of biological chemistry *278*, 8826-8836.

Yin, H., Price, F., and Rudnicki, M.A. (2013). Satellite cells and the muscle stem cell niche. Physiological reviews *93*, 23-67.

Yoshida, N., Yoshida, S., Koishi, K., Masuda, K., and Nabeshima, Y. (1998). Cell heterogeneity upon myogenic differentiation: down-regulation of MyoD and Myf-5 generates 'reserve cells'. Journal of cell science *111 (Pt 6)*, 769-779.

Zammit, P.S., Golding, J.P., Nagata, Y., Hudon, V., Partridge, T.A., and Beauchamp, J.R. (2004). Muscle satellite cells adopt divergent fates: a mechanism for self-renewal? The Journal of cell biology *166*, 347-357.

Appendix

SI Appendix, S20, is not available with this version

Figures

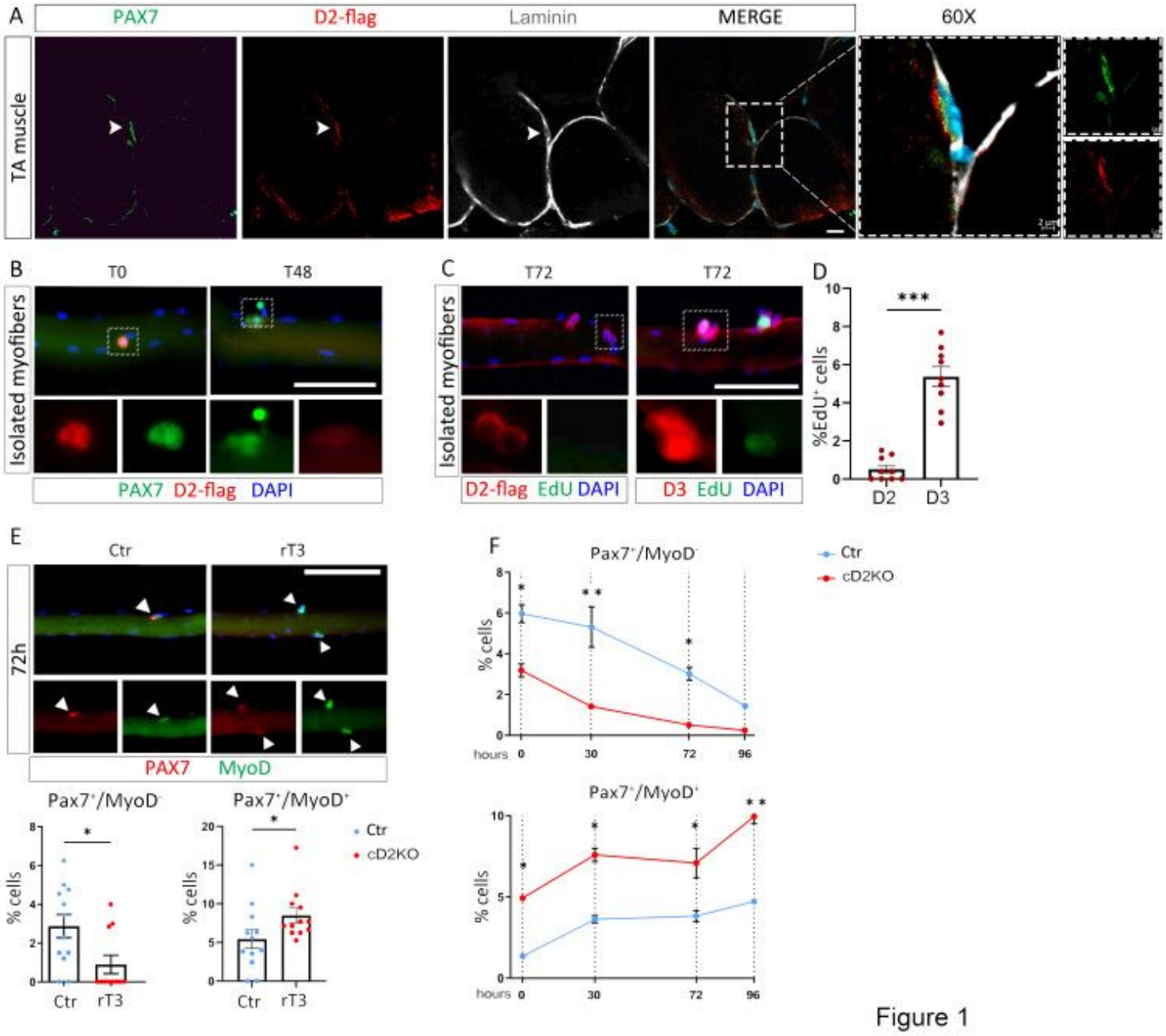

Figure 1

Figure 1

D2 is highly expressed in quiescent MuSCs.

A) Representative immunofluorescence (IF) of Pax7, D2 and laminin co-localization. Confocal images of Pax7 (green), D2-FLAG (red), Laminin (white) and DAPI (blue) expression on cryo-sections of tibialis anterior (TA) muscle of D2-FLAG mice (Pax7-D2 co-localizations are indicated with arrowhead) (Scale bar, 10 µm), to the right original magnification: 63x (Scale bar, 2 µm). (B) Single myofibers with associated MuSCs were fixed either immediately after isolation (0 hr) or after 48 hours in culture and then immunostained for Pax7 (green) and D2-FLAG (red) (Scale bar, 50 µm). (C) Representative IF staining for both D3 and D2 *versus* EdU images in cultured fibers at 72 hours (Scale bar, 50 µm) (n=3 mice in three individual experiments). (D) Quantification of percentage of EdU^+ cells of C. (E) Representative IF staining

of Pax7 (red) and MyoD (green) on isolated myofibers of D2-3xFLAG mice +/-rT3 treated at 72 hours. (Scale bar, 100 µm), quantification of percentage of positive cells (bottom) (Ctr n=4; rT3 n=4 mice in three separate experiments). (F) Quantification of the percentage of $Pax7^{+}/MyoD^{-}$, $Pax7^{+}/MyoD^{+}$ cells on isolated myofibers after TAM induction of Ctr ($Tg:Pax7^{creERT2+/+}; D2^{fl/fl}$) and cD2KO mice ($Tg:Pax7^{creERT2/+}; D2^{fl/fl}$) at different times (Ctr n=5; cD2KO n=4 mice in three individual experiment). In (D) and (E), data are represented as average ± SEM; *p < 0.05, **p < 0.01, ***p < 0.001 using a Mann-Whitney test when comparing two conditions. In (F) data are represented as average ± SEM; *p < 0.05, **p < 0.01, ***p < 0.001 using a 2way ANOVA when comparing multiple conditions.

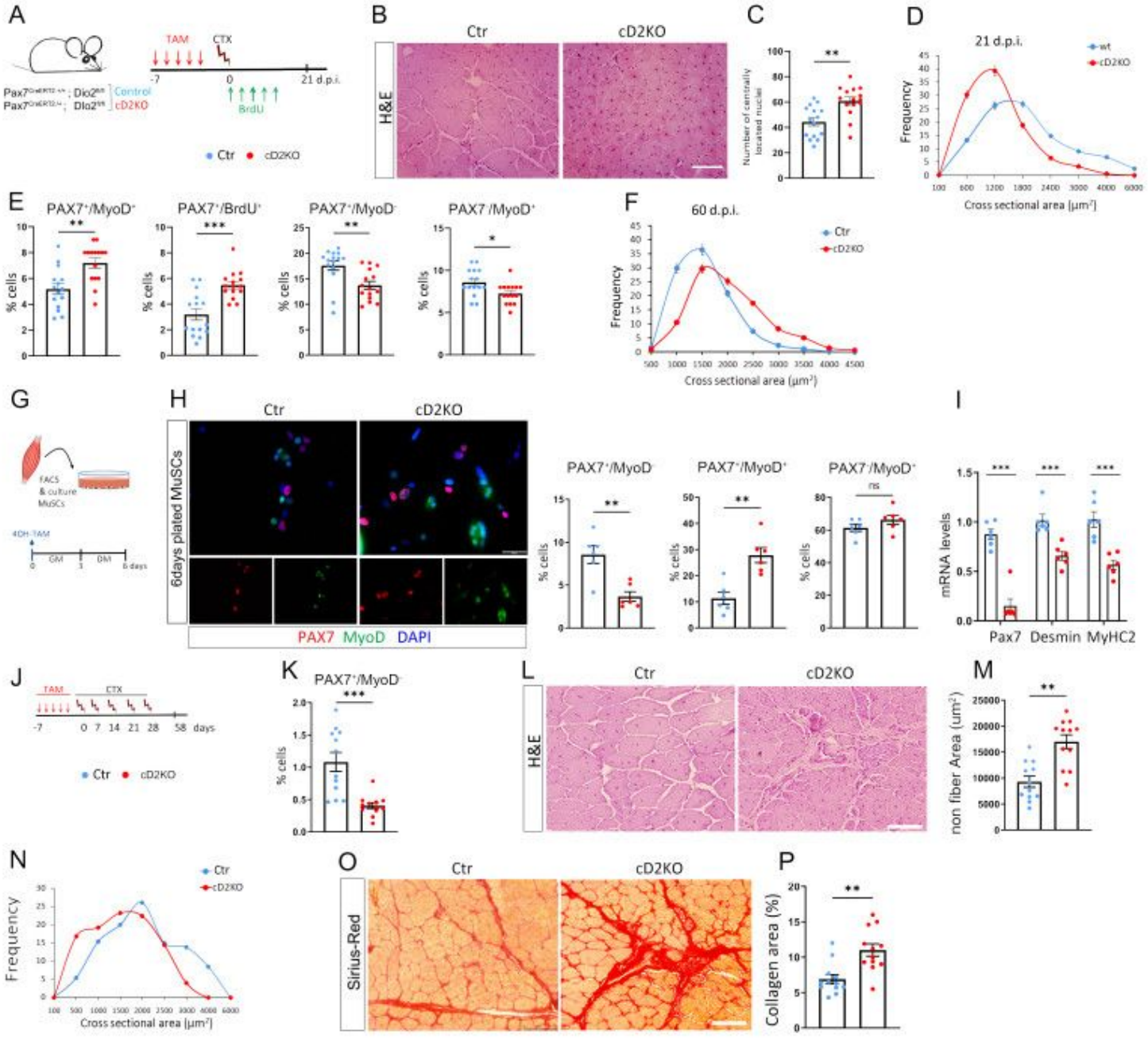

Figure 2

Figure 2

D2-depletion in quiescent MuSCs alters regeneration and self-renewal.

A-E, Schematic diagram of the experimental design (A). H&E staining of the TA sections from Ctr and cD2KO mice after TAM induction (Scale bar, 100 µm) (B). Percentage of centrally located nuclei (C). Quantification of the cross-sectional area of TA sections (D). Percentage of positive cells by double staining Pax7/MyoD and Pax7/BrdU (Ctr n=5; cD2KO n=5 in three separate experiments) (E).

(F) CSA analysis of TA sections from cD2KO (Tg:$Pax7^{creERT2/+}$; $D2^{fl/fl}$; $R26^{mTmG}$) and Ctr (Tg:$Pax7^{creERT2/+}$; $D2^{+/+}$; $R26^{mTmG}$) adult mice 60 days after CTX-injection.

G-I, Schematic design of the "*reserve experiment*". MuSCs isolated from cD2KO were plated in the presence or absence of 1µM 4OH-TAM and harvested 6 days thereafter (G). Representative immunostaining of Pax7 (red) and MyoD (green) (Scale bar, 200 µm), and percentage of positive cells (right) (H). Pax7, Desmin and MyHC2 mRNA levels were evaluated by qRT-PCR (I) (Ctr n=3; cD2KO n=3 in two separate experiments).

J-P, Schematic experiment of multiple CTX Pax in cD2KO and Ctr mice (J). Percentage of $Pax7^{+}$/$MyoD^{-}$ positive cells by IF (K). H&E of TA sections (Scale bar, 75 µm) (L). Percentage of non-myofiber tissue over the total section area (M). Quantification of the CSA (N). Representative Sirius-red staining of TA sections (Scale bar, 75 µm) (O). Percentage of collagen area (P). Ctr n=4; cD2KO n=4 mice in three independent experiments. In (C), (D), (E), (F), (H), (I), (K), (M), (N) and (P) data are represented as average ± SEM; *p < 0.05, **p < 0.01, ***p < 0.001 using a Mann-Whitney test when comparing two conditions, and 2way ANOVA when comparing multiple conditions.

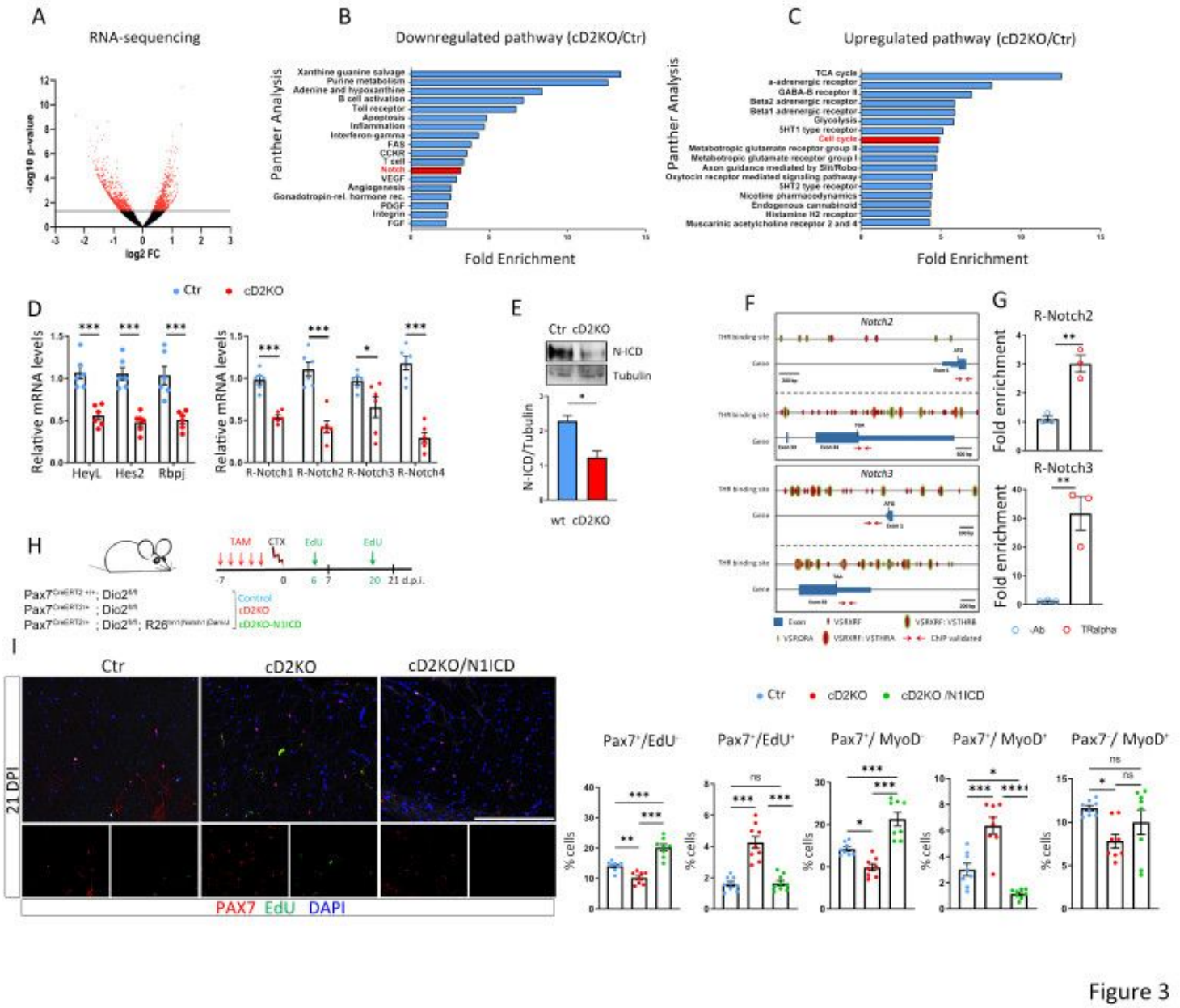

Figure 3

Figure 3

D2 is required for the maintenance of quiescence by sustaining the Notch pathway.

A-C, Volcano plot showing differences in the mRNA expression of qMuSCs from cD2KO and Controls. The negative log10 p-value (y-axis) and log2 fold change (FC; x-axis) are plotted for transcripts detected by RNA-seq analysis (gray line indicate p-value <0.05; n=3 biological replicates) (A). The most significant downregulated Panther (Protein Analysis Through Evolutionary Relationships) pathways (B). The most significant up-regulated Panther pathways (C).

D-E, mRNA levels of Notch targets (Hey-L, Hes2 and Rbpj) and Notch receptors (1-2-3-4) in Ctr and cD2KO qMuSCs isolated by FACS and measured by qRT-PCR. (Ctr n=3; cD2KO n=3 mice in two independent

experiments) (D). Protein levels of NICD measured by western blot. Tubulin served as a loading control. The graph on the right shows the quantification of NICD/tubulin (E).

(F) The 3' and 5' flanking regions of the mouse Notch2 and Notch3 genes. (G) C2C12 cells were processed for ChIP using THR-alpha and isotype control antibodies, followed by qRT-PCR of Notch2 and Notch3 receptors. The Data are normalized for background levels and input chromatin for each sample. H-I, Diagram of rescue experiment *in vivo* (H). Representative IF of Pax7/EdU in TA sections from Ctr, cD2KO and cD2KO/N1ICD mice harvested 21 days after CTX-injection (Scale bar, 200µm) (I). Percentage of positive cells for Pax7/EdU, and Pax7/Myod (image not shown) (right). Ctr n=4; cD2KO n=4 cD2KO-N1ICD n=4 mice in two independent experiments. In (D), (E), (G), (I) data are represented as average ± SEM; *p < 0.05, **p < 0.01, ***p < 0.001 using a Mann-Whitney test when comparing two conditions, and one-way ANOVA when comparing multiple conditions.

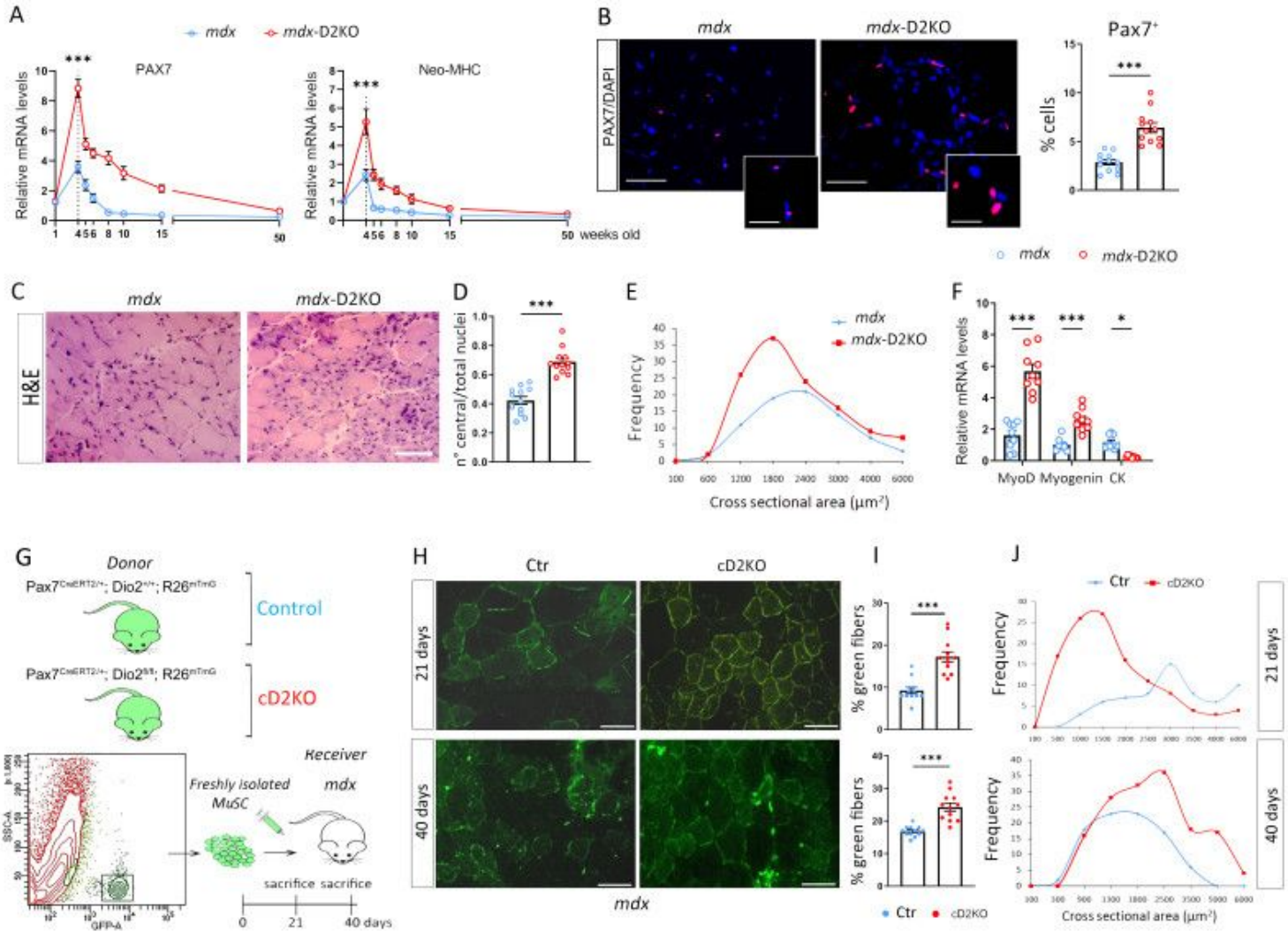

Figure 5

Figure 5

Phenotype's characterization of mdx-D2KO mice and xenograft studies into mdx mice.

(A) Pax7 and neo-MHC mRNA levels from Ctr and total *mdx*-D2KO mice were measured by qRT-PCR at different time points.

B-F, Representative IF and its quantification (right) of Pax7/DAPI of TA sections from Ctr and total *mdx*-D2KO mice 4 old weeks (Scale bar, 100 µm and 50 µm) (B). Representative H&E staining (scale bar, 100 µm) (C). Percentage of centrally located nuclei (D). Quantification of the cross-sectional area (E). mRNA Myogenin, MyoD and Creatin Kinase levels were measured by qRT-PCR (F). *mdx* n= 4; *mdx*-D2KO n=4, of three individual experiments.

G-J, Experimental design of FACS-isolated MuSCs from Ctr (Tg:Pax7$^{creERT2/+}$; D2$^{+/+}$; R26^{mTmG}) and cD2KO (Tg:Pax7$^{creERT2/+}$; D2$^{fl/fl}$; R26^{mTmG}) mice transplanted in the left and right TA muscles respectively in *mdx*-mice, which were sacrificed 21 and 40 days post-xenograft (G). Green epifluorescence fibers into *mdx* mice (Scale bar,100 µm) (H). Percentage of GFP fibers (green) 21 (top) and 40 days (bottom) following transplantation (I). Cross-sectional area of green fibers after 21 and 40 days from engraft (J). Ctr n= 4; cD2KO n=4 receiver mdx mice for three independent experiments. In (A), (B), (D), (E), (F), (I) and (J) data are represented as average± SEM; *p < 0.05, **p < 0.01, ***p < 0.001 using a Mann-Whitney test when comparing two conditions, and 2way ANOVA when comparing plus conditions.

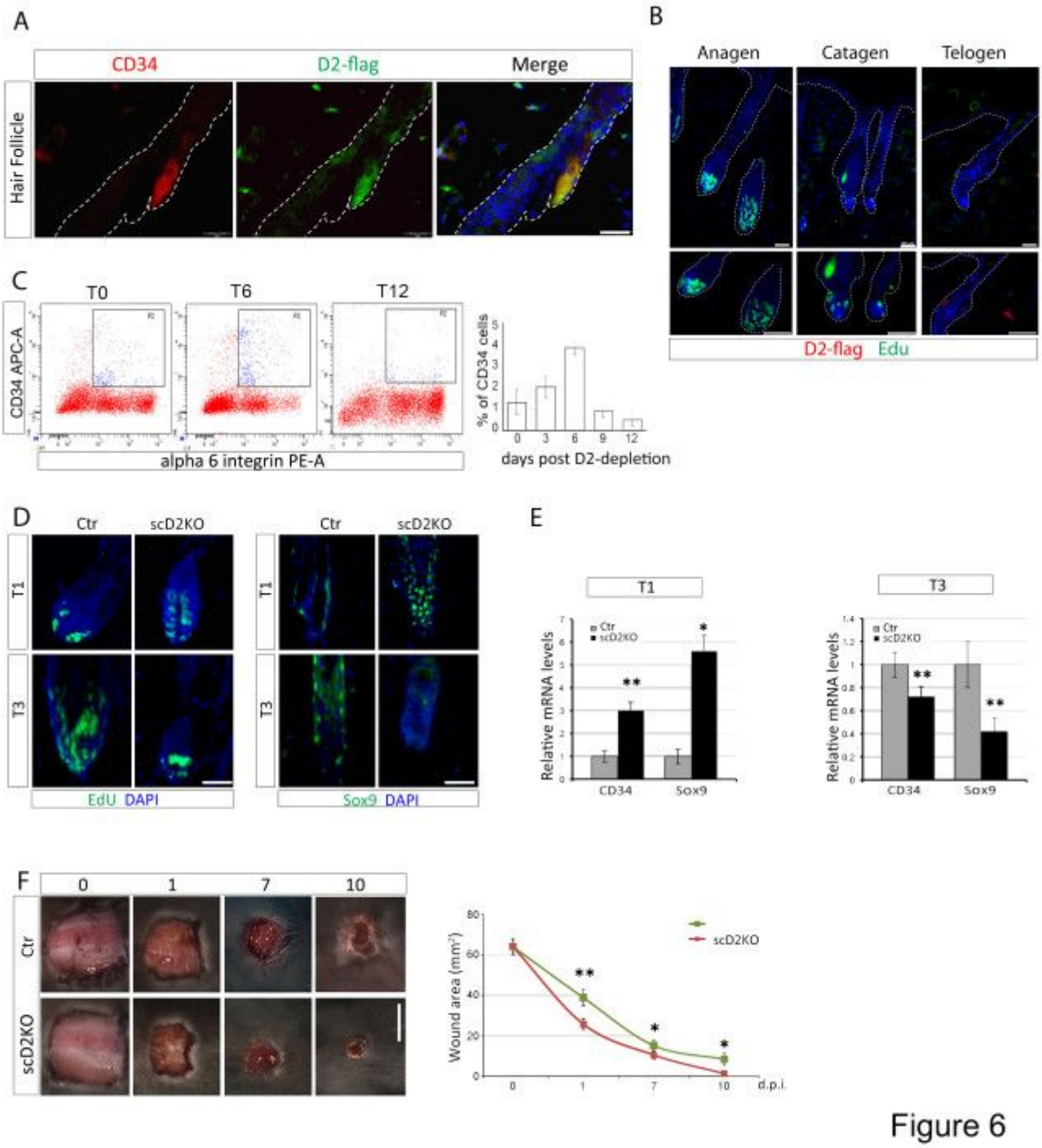

Figure 6

Figure 6

Analysis and functional characterization of D2 expression in mouse skin

(A) Representative IF co-staining of CD34 (red) and D2-FLAG (green) in the hair follicle (Scale bar, 40 μm). (B) Representative IF of EdU and D2 positive (green) cells during the hair follicle cycle (scale bar 50 μm (top), 20 μm (bottom). (C) Percentage of α6-integrin^{+}/CD34^{+} cells was evaluated by FACS analysis from epidermis of scD2KO at 0 (T0), 6 (T6) and 12 days (T12) after TAM-induced D2 depletion. D-E, EdU/DAPI

and Sox9/DAPI IF co-staining in the hair follicle after one (T1) and three (T3) consecutive shavings in scD2KO and Ctr mice (D). CD34 and Sox9 mRNA levels were measured by qRT- PCR (E).

(F) Wound healing experiment in scD2KO and Ctr mice following 7 days upon TAM- treatment. Representative images of the area at 0, 1, 7 and 10 days following the wound. Wound area was calculated by the Cell*F Olympus Imaging Software (Scale bar, 1 cm). Data are represented as average ± SEM; *p < 0.05, **p < 0.01, ***p < 0.001 using a Mann-Whitney test when comparing two conditions, and multiple T-test.

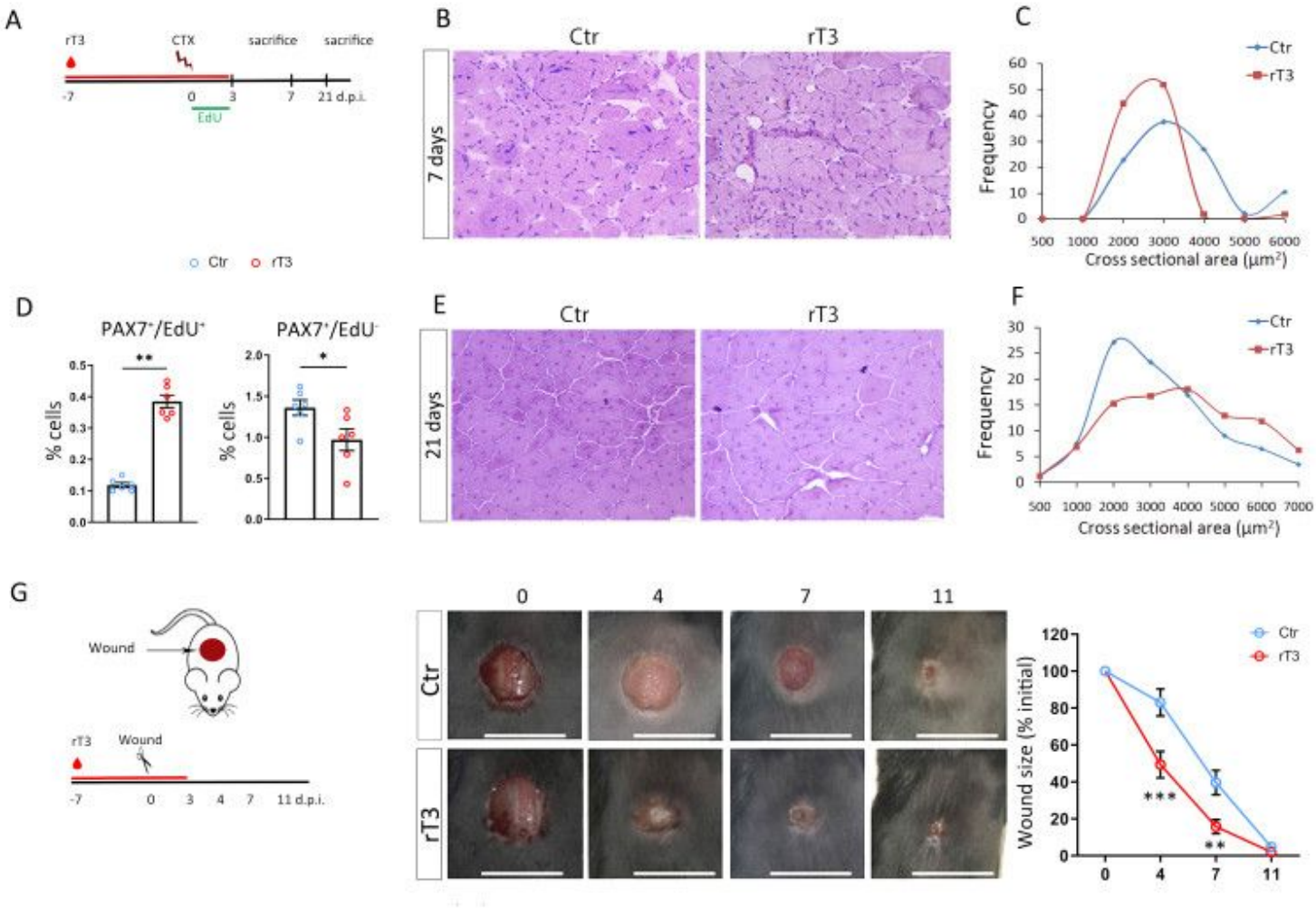

Figure 7

Figure 7

rT3 as a therapeutic agent to enhance expansion of activated precursor cells.

(A) Scheme of the experimental design. B-D Representative H&E from TA sections from rT3-treated and Ctr mice sacrificed 7 days after CTX-injury (Scale bar, 50µm) (B). Quantification of the CSA (C). Percentage of Pax7/EdU positive cells (D) (Ctr n=3; rT3 n=3 mice in two individual experiments).

E-F, Representative H&E from rT3-treated and Ctr mice sacrificed 21 days after injury (Scale bar, 50µm) (E). Quantification of the CSA (F).

(G) Diagram of the experimental design and representative images of wound healing in mice treated with rT3 versus control. Quantification of wound closure is presented as the mean of the percent of the initial wound size (right) (n =4 each group in four independent experiment) (Scale bar 1cm). Data are represented as average ± SEM; *p < 0.05, **p < 0.01, ***p < 0.001 using a Mann-Whitney test when comparing two conditions, and 2way ANOVA when comparing plus conditions.

Supplementary Files

This is a list of supplementary files associated with this preprint. Click to download.

- S1.pdf
- S2.pdf
- S3.pdf
- S4.pdf
- S5n.pdf
- S6.pdf
- Tab.S1.docx
- Tab.OLIGOS2.docx